Development of a Brain Metastatic Canine Prostate Cancer Cell Line

Nanda K. Thudi,[1] Sherry T. Shu,[2] Chelsea K. Martin,[2] Lisa G. Lanigan,[2] Murali V.P. Nadella,[2] Adrie Van Bokhoven,[3] Jillian L. Werbeck,[2] Jessica K. Simmons,[2] Sridhar Murahari,[4] William C. Kisseberth,[4] Matthew Breen,[5] Christina Williams,[5] Ching-Shih Chen,[6] Laurie K. McCauley,[7] Evan T. Keller,[8] and Thomas J. Rosol[2]*

[1]*Department of Radiation Oncology, University of Alabama, Birmingham, Alabama*
[2]*Department of Veterinary Biosciences, The Ohio State University, Columbus, Ohio*
[3]*Department of Pathology, University of Colorado Health Sciences Center, Aurora, Colorado*
[4]*Department of Veterinary Clinical Sciences, The Ohio State University, Columbus, Ohio*
[5]*Department of Molecular Biomedical Sciences, College of Veterinary Medicine, North Carolina State University, Raleigh, North Carolina*
[6]*Division of Medicinal Chemistry and Pharmacognosy, College of Pharmacy, The Ohio State University, Columbus, Ohio*
[7]*Department of Periodontics and Oral Medicine, School of Dentistry, University of Michigan, Ann Arbor, Michigan*
[8]*Departments of Urology and Pathology, School of Medicine, University of Michigan, Ann Arbor, Michigan*

BACKGROUND. Prostate cancer in men has a high mortality and morbidity due to metastatic disease. The pathobiology of prostate cancer metastasis is not well understood and cell lines and animal models that recapitulate the complex nature of the disease are needed. Therefore, the goal of the study was to establish and characterize a new prostate cancer line derived from a dog with spontaneous prostate cancer.

METHODS. A new cell line (Leo) was derived from a dog with spontaneous prostate cancer. Immunohistochemistry and PCR were used to characterize the primary prostate cancer and xenografts in nude mice. Subcutaneous tumor growth and metastases in nude mice were evaluated by bioluminescent imaging, radiography and histopathology. In vitro chemosensitivity of Leo cells to therapeutic agents was measured.

RESULTS. Leo cells expressed the secretory epithelial cytokeratins (CK)8, 18, and ductal cell marker, CK7. The cell line grew in vitro (over 75 passages) and was tumorigenic in the subcutis of nude mice. Following intracardiac injection, Leo cells metastasized to the brain, spinal cord, bone, and adrenal gland. The incidence of metastases was greatest to the central nervous system (80%) with a lower incidence to bone (20%) and the adrenal glands (16%). In vitro chemosensitivity assays demonstrated that Leo cells were sensitive to Velcade and an HDAC-42 inhibitor with IC_{50} concentrations of 1.9 nm and 0.95 μm, respectively.

CONCLUSION. The new prostate cancer cell line (Leo) will be a valuable model to investigate the mechanisms of the brain and bone metastases. *Prostate 71: 1251–1263, 2011.*

KEY WORDS: **prostate cancer; brain metastasis; spinal cord metastasis; dog; canine; bone metastasis**

Grant sponsor: National Cancer Institute; Grant number: 2P01 CA93900; Grant sponsor: The Ohio State University College of Veterinary Medicine; Grant number: 520026.

*Correspondence to: Thomas J. Rosol, DVM, PhD, 1925 Coffey Road, Columbus, OH 43210. E-mail: rosol.1@osu.edu
Received 20 July 2010; Accepted 16 December 2010
DOI 10.1002/pros.21341
Published online 14 February 2011 in Wiley Online Library (wileyonlinelibrary.com).

INTRODUCTION

Prostate cancer is the most commonly diagnosed cancer in men accounting for 25% of all cancers in the United States [1]. Prostate cancer in advanced stages has a high incidence of bone metastases that causes severe skeletal complications resulting in morbidity and mortality. Dogs are the only non-human mammals that develop spontaneous prostate cancer, which shares many characteristics in clinical presentation and pathogenesis of the disease as in men [2]. In addition, dogs also have extensive genomic homology with humans, and recent sequencing of the dog genome and development of dog gene arrays make the dog an invaluable animal model to study the pathogenesis of prostate cancer in spontaneous or experimental settings [3]. Previously, our laboratory established the ACE-1 canine prostate cancer cell line that metastasizes almost exclusively to bone and induces mixed osteoblastic and osteolytic lesions in nude mice similar to bone metastases in men with prostate cancer [4].

Although bone is the primary site of metastases in prostate cancer, metastases also occur in lymph nodes, brain, lung, adrenal gland, and liver [5–7]. Soft tissue metastases, alone or in combination with bone metastases, were detected in 33% of prostate cancer patients with metastases [8]. Brain metastases occurs in a small percentage of patients (1%), but is often a terminal event. Median survival rate is 1 month in untreated patients with brain metastases, 3.5 months in patients who received radiotherapy and 9 months in patients who had stereotactic radiosurgery [9]. Although brain metastases are uncommon in prostate cancer, the annual incidence of more than 150,000 cases of brain metastases from other cancers was reported in the US [10]. It is important to develop new therapies for patients with brain metastases due to their serious consequences. Therefore, understanding the molecular pathogenesis of prostate cancer brain metastases will facilitate the development of novel treatment strategies.

Although numerous prostate cancer cell lines have been developed, few cell lines develop bone metastases and no cell lines have been reported to cause brain metastases [11]. Despite the fact that the DU145 cell line was developed from a brain metastasis from a human prostate cancer patient, these cells have not demonstrated the ability to metastasize to the brain in animal models [12]. Therefore, lack of prostate cancer cell lines that develop brain metastases have impeded studies of prostate cancer brain metastases.

In this investigation, we report the establishment of a novel dog prostate cancer cell line and its ability to metastasize to numerous sites in the nude mouse including brain, spinal cord, bone, and adrenal gland.

MATERIALS AND METHODS

Establishment of a canine prostate carcinoma cell line (Leo)

Tissue from a spontaneously arising prostate carcinoma was collected immediately following euthanasia of a tumor-bearing, 5-year-old, castrated male mixed breed dog and washed three times in DMEM/F12 (Invitrogen Corp., Carlsbad, CA) containing 50 μg/ml primocin (Invivogen, San Diego, CA) and minced into approximately 1 mm^3 pieces. The tissue pieces were digested in 500 units/ml of collagenase type 1 (Worthington Biochemical, Lakewood, NJ) in serum-free DMEM/F12 for 2 hr at 37°C on a rocker platform with gentle rocking. The digested tissue was washed three times with DMEM/F12 containing 50 μg/ml Primocin and 10% fetal bovine serum (FBS) (Invitrogen Corp.) and plated in a T-75 flask (Falcon; Becton-Dickinson, Franklin Lakes, NJ). Medium was changed every 3 days. Differential trypsinization was performed to eliminate the stromal cell contamination of epithelial cells once every 2 days by treating the cultures with 0.05% trypsin ethylenediamine-tetraacetic acid (EDTA) (Invitrogen Corp.). Detachment of the cells was monitored every 2 min to remove the stromal cells, which detached earlier than the epithelial cells. The first phase of detached cells (mostly stromal cells) was removed and the remaining epithelial cells were collected and replated.

Lentiviral yellow fluorescent protein-luciferase (YFP-Luc) vector production and transduction of Leo cell line

YFP-Luc lentiviral particles were produced by transient co-transfection of 293T cells with 10 μg packaging plasmid pCMVDR8.2, 2 μg envelope plasmid pMD.G and 10 μg transfer plasmid pHIVSIN-YFP-Luc using calcium phosphate (Sigma–Aldrich Co., St. Louis, MO) as described previously [13]. The virus supernatant was collected at 24 hr, filtered through a 0.2 μm filter, and stored at −80°C until use. Leo cells were transduced with the retroviral YFP-Luc dual reporter gene and 8 μg/ml polybrene by spin inoculation at 2700 rpm for 1 hr at 32°C and transferred to a cell culture incubator overnight. Cells were maintained in DMEM/F12 medium containing 10% FBS and 50 μg/ml Normocin (Invivogen).

Subcutaneous and intracardiac left ventricular inoculation of Leo cells in nude mice

Subcutaneous (N = 10) and intracardiac (N = 25) injections of Leo YFP-Luc cells were performed in

6-week-old male nu/nu mice (National Cancer Institute, Frederick, MD) under general anesthesia with a 3% isoflurane (Abbott Laboratories, North Chicago, IL)-oxygen mixture. All the animal experimental procedures were approved by The Ohio State University Institutional Laboratory Animal Care and Use Committee. Ten million Leo cells suspended in 250 μl of phosphate-buffered saline (PBS) (Invitrogen) were injected subcutaneously over the dorsal interscapular area of mice. Subcutaneous tumor growth in mice was measured weekly using Vernier calipers and bioluminescent imaging (BLI) and sacrificed after 6 weeks. Left ventricular cardiac injections were performed with 1×10^5 cells suspended in 100 μl of PBS using a 26 gauge needle. Subcutaneous and metastatic tumor growth and incidence were monitored using BLI (see below). Immediately after intracardiac injection of $Leo^{YFP\text{-}Luc}$ cells, a diffuse BLI signal originating from the tumor cells throughout the entire body was considered successful left ventricular injection. Mice were sacrificed after 4 weeks.

Bioluminescent imaging

Mouse BLI was performed using an in vivo imaging system (IVIS 100, Caliper Life Sciences, Hopkinton, MA) as described previously [11]. Briefly, 4.5 mg d-luciferin (Caliper Life Sciences) dissolved in 150 μl PBS was injected intraperitoneally into mice and imaging was carried out in an imaging chamber under general anesthesia with a 1.5% isoflurane – oxygen mixture until peak photon signal was attained. The photon signal intensity was quantified using LivingImage software version 2.50 (Caliper Life Sciences).

In vitro growth rate

Cells (5×10^5) from passage 70 were plated in 10 cm plates (Falcon) in quadruplicate in DMEM/F12 medium with 10% FBS and 50 μg/ml Normocin (Invivogen) and incubated at 37°C in 5% CO_2. The cells were harvested using 0.25% trypsin (Fisher Scientific, Pittsburgh, PA) at 24, 48, and 72 hr after plating and counted with an automated cell counter (Nexcelom Bioscience, Lawrence, MA) using trypan-blue dye exclusion to count live and dead cells. Doubling time was calculated using the formula: $(t_2 - t_1) \times \log(n_2)/\log(n_2/n_1)$, where n is the cell number at time points (t) [14].

Radiography of mice

High-resolution radiographic images of mice were obtained using a Faxitron laboratory radiography system LX-60 (Faxitron X-ray Corp., Wheeling, IL) at 30 KVp for 10 sec on day 28.

Histopathology and immunohistochemistry

Complete necropsies were performed on the mice and tissues were fixed in 10% neutral-buffered formalin at 4°C for 24 hr. Bones were decalcified in 10% EDTA (pH 7.4) for 2 weeks at 4°C and embedded in paraffin. The specimens were sectioned (5 μm) and were either stained with hematoxylin and eosin (H&E) or evaluated by immunohistochemistry using human antibodies for the presence of cytokeratin (CK)-5/14, 8, 18, 7, vimentin, androgen receptor (AR) and prostate specific antigen (PSA) to characterize the prostate carcinoma cells (see Table I for a list of primary antibodies). Sections were deparaffinized in xylene (Hemo-De, Fisher Scientific, Bay Shore, NY) by two 3-min washes and rehydrated in 100%, 95%, and 70% ethanol sequentially for 3 min and rinsed in water. Endogenous peroxidase activity was removed using 3% H_2O_2 (Dako Corp., Carpinteria, CA) for 5 min at room temperature (RT) and washed in PBS for 15 min. To block non-specific binding of proteins, sections were incubated in Protein Block (Dako Corp.) for 15 min at RT and rinsed in PBS. Antigen retrieval was performed using target retrieval solution and heated for 30 min in an oven at 60°C. Primary antibodies (see Table I) were added to sections and incubated at RT for 30 min and sections were washed three times for 5 min in PBS/0.05% Tween. After washing, sections were incubated either with universal biotinylated goat anti-mouse or

TABLE I. Anti-Human Antibodies Used for Immunohistochemistry of the Primary Prostate Carcinoma

Antibody	Species	Clone	Company	Dilution
MA903 (CK5/14)	Mouse	34βE12	Enzo Life Sciences, Farmingdale, NY	1:100
CK18	Mouse	KS-B17.2	Sigma–Aldrich, St Louis, MO	1:100
CK8	Mouse	4.1.18	Chemicon, Temecula, CA	1:30
Vimentin	Mouse	Clone V9	Cell Marque, Hot Springs, AR	1:50
CK7	Mouse	OV-TL12/30	Dako Corporation, Carpinteria, CA	1:40
AR	Rabbit	N-20	Santa Cruz Biotechnology, Inc, Santa Cruz, CA	1:500
PSA	Rabbit	Polyclonal	Dako Corporation, Carpenteria, CA	1:150

biotinylated goat anti-rabbit IgG secondary antibody (1:250 dilution in protein block reagent) for 30 min at RT and followed by three 5-min washes in PBS/0.05% Tween. Sections were incubated with avidin–biotin complex for 30 min according to the manufacturer's instructions (Vectastain ABC Kit, Vector Laboratories, Inc., Burlingame, CA). To visualize the peroxidase activity, sections were incubated with 3,3′-diaminobenzidine reagent (1:50 concentrate:reaction buffer) for 5 min at RT and rinsed in distilled water. The slides were counterstained with hematoxylin for 1 min, dried, and coverslipped with xylene-based mounting media.

RNA extraction and reverse transcription-polymerase chain reaction (RT-PCR)

Total RNA was extracted from Leo cells, Ace-1 dog prostate cancer cells [4], dog transitional cell carcinoma (TCC) cells [15] and dog brain using Trizol reagent according to manufacturer's protocol (Invitrogen). Total RNA (2.5 μg) was reverse transcribed using the Superscript II First Strand cDNA synthesis kit (Invitrogen) and RT-PCR was performed for parathyroid hormone-related protein (PTHrP), matrix metalloproteinase (MMP-9), vascular endothelial growth factor (VEGF), beta2-microglubulin (B2M), receptor activator of NF-kappaB ligand (RANKL), osteoprotegerin (OPG), nerve growth factor (NGF), low-affinity nerve growth factor receptor (LNGFR), and neurotrophin tyrosine receptor kinase 1 (NTRK1) using canine-specific primers (Table II).

PTHrP immunoradiometric assay

PTHrP concentrations were measured in the Leo cell conditioned medium at 0, 6 12, 24 hr after the addition of serum-containing medium. Negative control medium was not conditioned by any cells. PTHrP concentration was quantified using a two-site immunoradiometric assay (DSL, Webster, TX) specific for PTHrP 1-80 using antibodies to the N-terminal region (amino acids 1–40) and mid-region (amino acids 57–80) according to manufacturer's instructions.

TABLE III. Incidence of Leo$^{YFP\text{-}Luc}$ Metastases by Anatomic Location at 28 days Following Intracardiac Injection

Site of metastasis	Incidence
Total mice with metastases	23/25
Brain	19/25
Spinal cord	2/25
Bone	5/25
Adrenal gland	4/25

Analysis of Leo genomic imbalances by fluorescent in situ hybridization (FISH)

Cells were grown to ~80% confluence and 50 ng/ml of Karyomax (Invitrogen) were added to the medium and incubated at 37°C for 4 hr. Chromosome preparations were generated following conventional procedures of hypotonic treatment and fixation in 3:1 methanol:glacial acetic acid. Chromosome preparations were counterstained with 80 ng/ml 4′,6-diaminidino-2-phenylindole (DAPI) and mounted in antifade solution (Vectashield, Vector Laboratories). Images were acquired with a fluorescence microscope (Axioplan 2ie, Zeiss) equipped with a DAPI filter set and a cooled CCD camera (CoolSnapHQ, Photometrics, Tuscon, AZ) both driven by dedicated software (SmartCapture 3, Digital Scientific, Cambridge, UK). The digital image of each DAPI stained metaphase spread was processed using a high-pass spatial filter to reveal enhanced DAPI bands [16,17]. Chromosome counts were obtained from 50 metaphase preparations. To identify the position of the centromeres of the chromosomes, two BAC clones (330E21 and 326K03) from the CHORI-82 BAC library, which have been

TABLE II. Dog-Specific Primers Used for RT-PCR Amplification

Gene	Forward primer (5′–3′)	Reverse primer (5′–3′)
PTHrP	AGCTCGGCCGCCGGCTCAA	GGAAGAATCGTCGCCGTAAG
MMP9	TGCAAAGTGAACATCTTCGACGCC	AGAAAGTCTTCTTGGTGAGCCCGT
VEGF	ATCGAGTACATCTTCAAGCCATCC	CTATGCTGCAGGAAACTCATCTCC
RANKL	AGGTTGGGCCAAGATCTCCAACAT	TCAGCTGAAGATACTCTGTGGCGA
OPG	AACTCATGACAATGTATGCTCTGG	ACGCTGAGCCAATTAGGAGT
NGF	GAGAAACGCTCACTGGGTTC	TGCTCCTGTGAGTCCTGTTG
LNGFR	CTGCAAAGCCTGCAATCTG	CCACCTCTTGAAGGCAATGT
NTRK1	TAGGTGGCAGTTCCTTGTCC	GAACTTGCGGTAGAGGATGC
B2M	CTTGCTCCTCATCCTCCTC	TGACACGTAGCAGTTCAG

shown previously to hybridize to all autosomal centromeres of the canine genome [18], were labeled with SpectrumGreen-dUTP and hybridized to chromosome preparations of this cell line according to routine procedures [19].

Canine genome 2.0 arrays

RNA was extracted from Leo cells and purified with Absolutely RNA® Miniprep Kit (Stratagene, La Jolla, CA). RNA was assayed for quality using Agilent RNA 6000 Nano Assay (Santa Clara, CA). Only samples exhibiting minimal degradation as evidenced by RNA integrity numbers >8 were used for mircoarrays. Three samples at three separate passages were selected and array analysis with GeneChip Canine 2.0 Genome Arrays (Affymetrix, Santa Clara, CA) was performed at OSU's Comprehensive Cancer Center Microarray Shared Resource. Background correction and normalization was performed to avoid technical bias, and gene expression level was summarized over the probeset using the RMA method. A Linear model was performed to detect differentially expressed genes [20]. In order to improve the estimates of variability and statistical tests for differential expression, variance shrinkage method was employed for this study [21]. The significance level was adjusted by controlling the mean number of false positives [22].

Data analysis

The half maximum inhibitory concentrations (IC_{50}) of the drugs were calculated using Calcusyn software (Biosoft, Cambridge, UK).

RESULTS

Histopathology of the prostate carcinoma

In the dog, the normal prostate gland was replaced by a highly invasive carcinoma consisting of multiple lobules of polygonal to columnar cells arranged in large sheets of cells and nests of cells separated by dense fibrous connective tissue (typical of the alveolar pattern of canine prostate cancer). Neoplastic cells had abundant cytoplasm with occasional cells containing a single, round, clear cytoplasmic vacuole, which displaced the nucleus (signet ring formation). Binucleate cells were often apparent and up to three nucleoli were present in the nuclei (Fig. 1A). Neoplastic tissue had regions of necrosis with secondary inflammation. The carcinoma invaded into the trigone region of urinary bladder and metastasized to the iliac lymph node, liver, lung, and right proximal tibia. The central nervous system was not examined since the dog had no neurologic clinical signs.

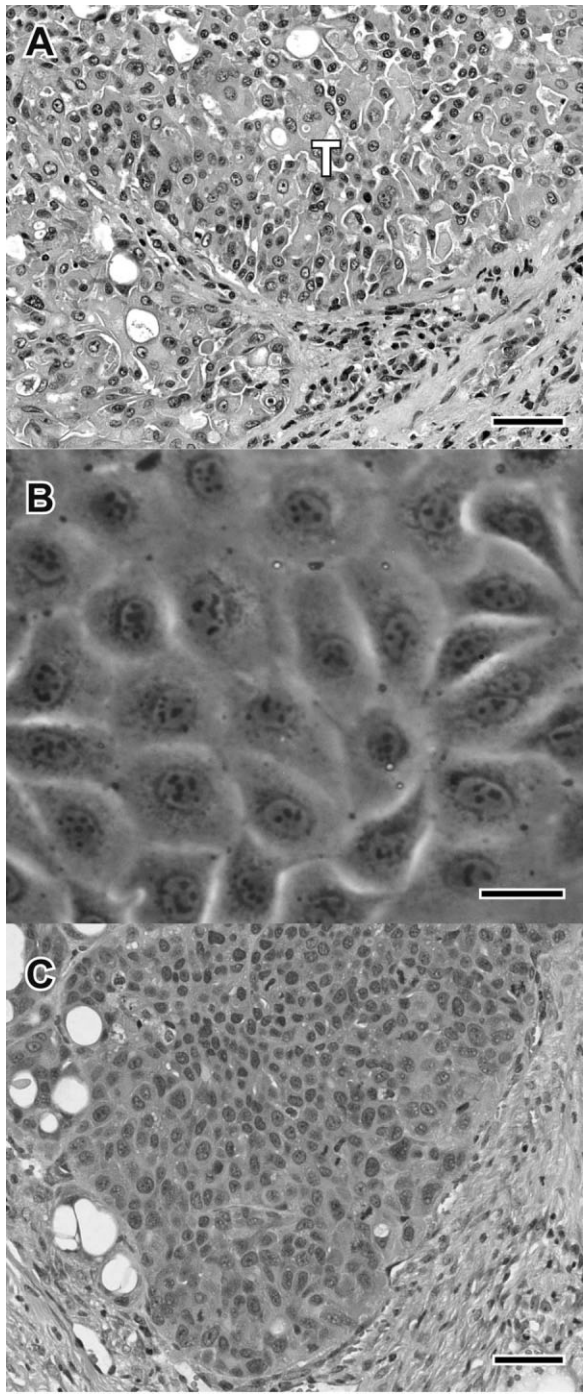

Fig. 1. Photomicrographs of primary prostate carcinoma, in vitro cell line (Leo) and subcutaneous xenograft. **A**: Photomicrograph of H&E-stained primary prostate carcinoma. Note the solid carcinoma consisting of multiple lobules of polygonal to columnar cells (alveolar pattern) separated by fibrous connective tissue. *Bar*, 50 μm. **B**: Phase contrast microscopy of Leo cells (passage 65). The polyhedral cells have a tightly packed cobblestone growth pattern. *Bar*, 20 μm. **C**: Photomicrograph of H&E-stained subcutaneous Leo xenograft. Tumors were multilobular with large polygonal cells. *Bar*, 50 μm.

Development of Leo prostate cancer cell Line

The prostate cancer cell line, Leo, was established from the primary prostate carcinoma tissue. The cell line has been passaged over 75 times in vitro. The cells grow in an anchorage-dependent manner in monolayer sheets with polyhedral cells exhibiting a tightly packed cobblestone growth pattern (Fig. 1B).

Subcutaneous growth of Leo prostate carcinoma cells

Leo cells injected into the subcutaneous region of nude mice formed tumors that average 0.8 cm^3 in 6 weeks (Fig. 4C). The microscopic appearance of the Leo subcutaneous xenografts was similar to the primary carcinoma. (Fig. 1C).

Immunohistochemistry of the primary prostate carcinoma

The primary prostate carcinoma was moderately positive for CK8 (Fig. 2A) and strongly expressed CK18 (Fig. 2B), which are markers of prostatic secretory cells. The cancer cells were negative for basal cell CK markers CK5 and 14 (data not shown). Previously it was reported that prostate cancer can originate from ductal cells in dogs and express the CK marker, CK7 [23,24]. The primary cancer cells expressed CK7 staining in the cytoplasm (Fig. 2C). AR, human PSA, and vimentin were not expressed by the carcinoma cells (Data not shown). Dog prostate glands do not express human PSA, but have a related kallikrein, arginine esterase (AE) [25]. The canine genomic array demonstrated that the Leo cells expressed AE at three different passages (passage 12, 13, and 14).

RT-PCR and PTHrP secretion of the Leo prostate cancer cell line

Leo cells expressed mRNA for MMP-9 and VEGF (Fig. 3), which have been reported to play an important role in the development of brain metastases [26,27]. RANKL and OPG were expressed by the Leo cells (Fig. 3) and might play a role in the bone metastases developed by Leo cells after intracardiac injection. Expression of PTHrP, NGF, LNGFR, and NTRK1 were not detectable. PTHrP concentrations in Leo cell conditioned media at different time points were similar to control medium without cells.

In vitro growth and in vivo tumorigenicity

Leo cells grew exponentially in vitro with a doubling time of approximately 38 hr under standard cell culture conditions (Fig. 4A). Leo cells were transduced with YFP-Luc to monitor in vivo growth. The $Leo^{YFP\text{-}Luc}$ cells were injected into the subcutis of nude mice to test their tumorigenicity. Subcutaneous tumor growth

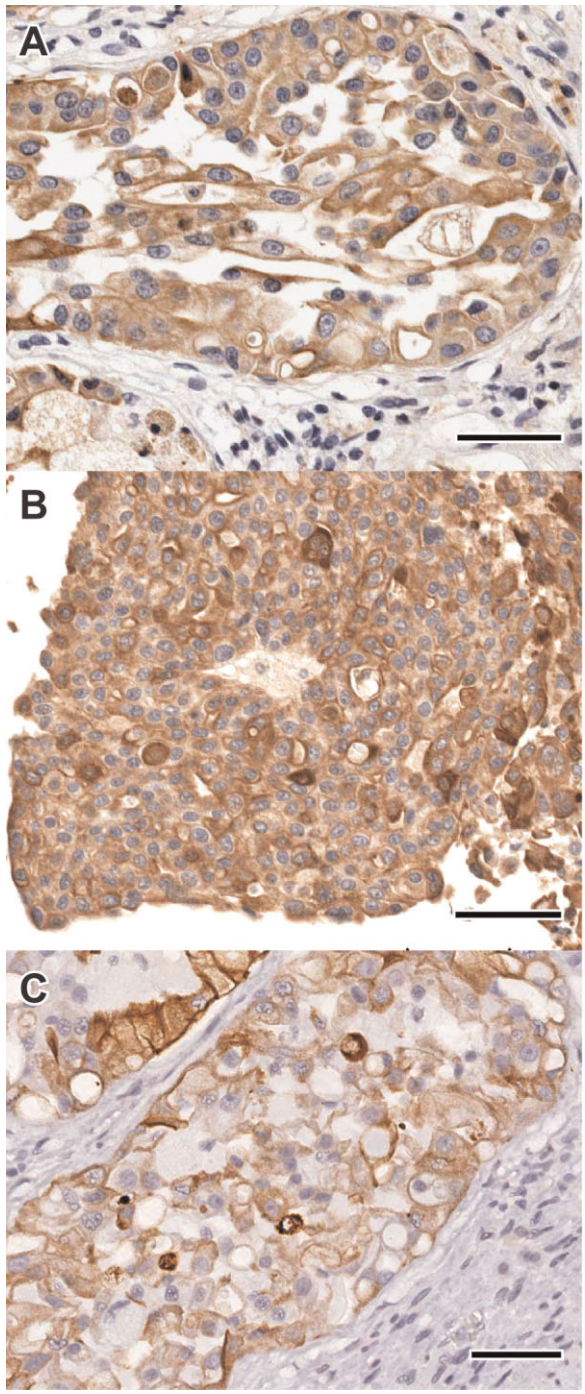

Fig. 2. Immunohistochemistry of the primary prostate carcinoma. **A**: CK8 staining in the cytoplasm was moderately positive. **B**: CK18 staining in the cytoplasm was strongly positive. **C**: CK7 staining in cytoplasm was moderately positive. *Bars*, 20 μm.

was detected in all mice (n = 10) and was progressive over 6 weeks (Fig. 4B and C).

Metastases of Leo cells in nude mice

Left ventricular intracardiac injections of $Leo^{YFP\text{-}Luc}$ were performed in 25 male nude mice in two separate

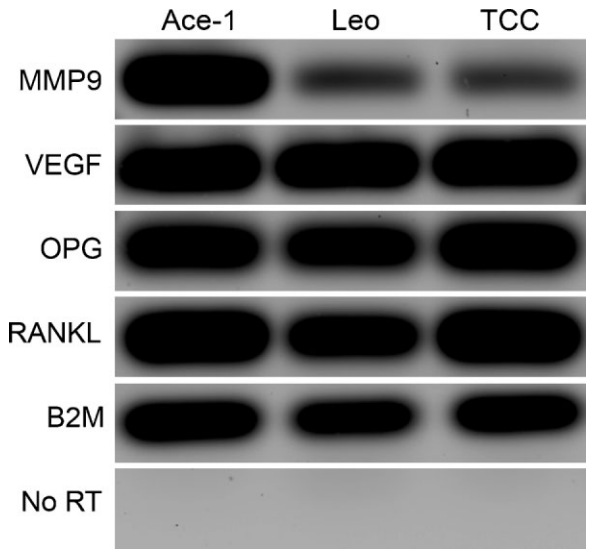

Fig. 3. mRNA expression of Leo cells. Expression of MMP-9, VEGF, OPG, RANKL mRNA were detected using RT-PCR in canine prostate cancer cells lines; Ace-1 and Leo and a dog TCC cell line. Expression of β2microglobulin was used as a control.

experiments. Metastatic ability of tumor cells was monitored weekly using BLI. At day 7, BLI signal was undetectable indicating that most injected Leo cells died. On day 14, metastatic foci were detected by BLI at different sites including the head, hind limbs, vertebrae and scapular region. BLI intensity of the metastatic foci increased at days 21 and 28. Metastases were detected in 23/25 mice. Mice were sacrificed on day 28 and ex vivo imaging of individual organs were performed immediately to localize the metastases. Metastases detected by BLI were confirmed by histopathological evaluation.

Histopathological analysis showed the presence of prostate carcinoma in the brain (19/25 mice), spinal cord (2/25 mice), adrenal gland (4/25), long bones (5/25), and scapula (1/25) (Table III). Leo cells most commonly metastasized to brain (Fig. 5A and B) when compared to other organs. Tumors in the brain ranged from 1 mm to 5 mm in diameter and multiple metastatic foci were observed in each brain section. Metastatic tumor in the brain and spinal cord (Fig. 5C and D) was most frequently located within the white matter. The brain and spinal cord metastases were expansile with compression of surrounding neurophil consistent with tumor size. Central necrosis and hemorrhage were features of larger tumors within the brain. Adrenal metastases replaced the medulla and cortex of the adrenal gland (Fig. 5E and F). In long bone metastases, such as tibia and femur, tumor cells caused osteolysis characterized by loss of cortical and trabecular bone in the metaphyseal region (Fig. 6A–C). The single

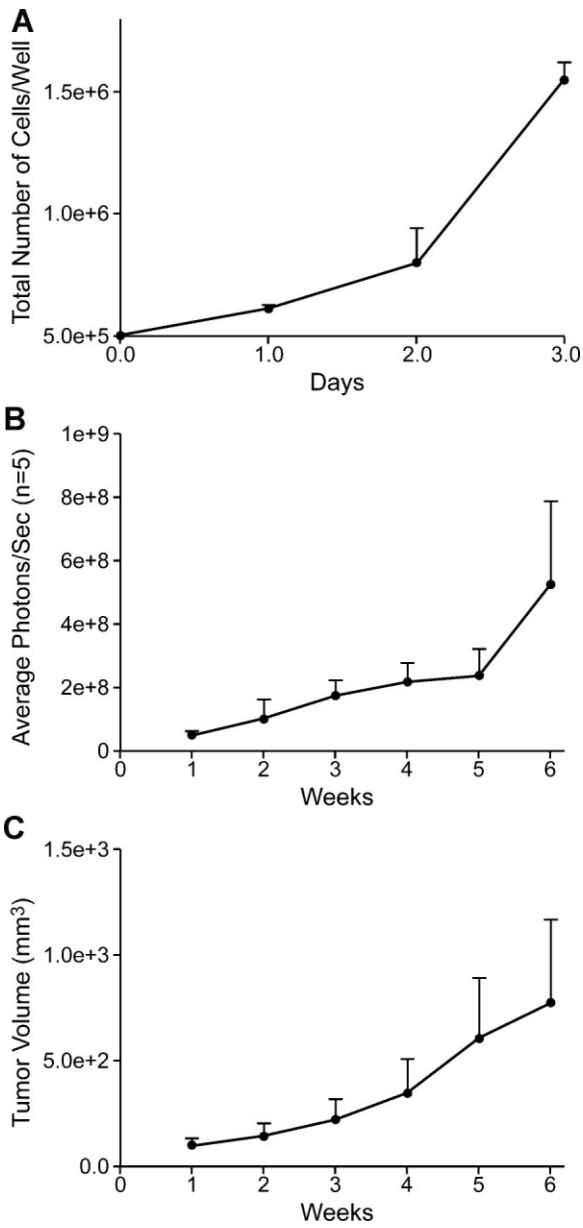

Fig. 4. In vitro and in vivo growth patterns of Leo cells. **A**: In vitro growth curve of Leo cells. Data presented as mean + standard deviation of four replicates. **B**: Graph represents the average intensity of the BLI signal measured at the indicated time points. **C**: Graph represents the average tumor volume. Data presented as mean + standard deviation of 10 mice.

metastatic lesion to the scapula was osteoblastic and consisted of tumor cells surrounding the scapular bone and containing large radiating bands (50 μm wide) of new woven bone proliferation lined by tall cuboidal osteoblasts (Fig. 6D–F).

In vitro chemosensitivity

The in vitro chemosensitivity of the Leo cells to different doses of calcitriol, piroxicam, (S)-HDAC-42

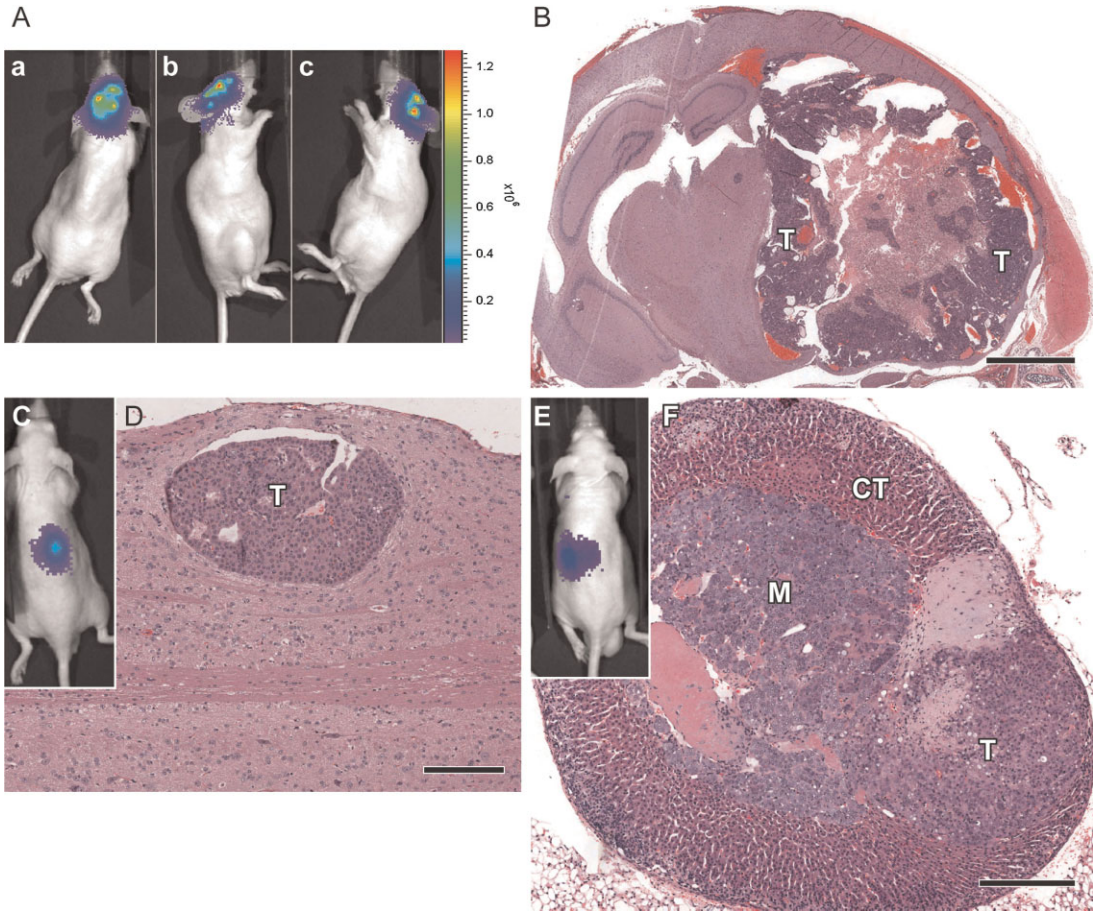

Fig. 5. In vivo BLI and histopathologic evaluation of nude mice 28 days following intracardiac injection of Leo$^{YFP\text{-}Luc}$ cells (**A**) was performed in ventral (a) and lateral (b,c) recumbency and demonstrated metastasis to the cranium. **B**: H&E-stained coronal section of brain revealed a large metastatic carcinoma (T, right side) with multiple small metastases in the brain parenchyma. BLI evaluation of spinal cord metastasis. *Bar*, 500 μm (**C**). Histopathologic evaluation (**D**) showed a metastatic carcinoma (T) in the white matter of spinal cord (H&E). *Bar*, 100 μm. BLI evaluation revealed a metastasis to the lumbar region (**E**), which was microscopically confirmed as an adrenal metastasis. *Bars*, 250 μm (**F**). Tumor cells are indicated by (T), adrenal cortex by (CT) and adrenal medulla by (M), H&E.

(Ar-42) and Velcade (bortezomib) was measured using the MTT assay at 72 hr. All the drugs inhibited cell growth in a dose-dependent manner. The half maximum inhibitory concentrations (IC_{50}) were calculated using Calcusyn software and were 6.5 μM for calcitriol (Fig. 7A), 1.9 nm for Velcade (Fig. 7B), 0.95 μm for (S)-HDAC-42 (Fig. 7C) and 518 μm for piroxicam (Fig. 7D). The in vitro IC_{50} concentrations of calcitriol and piroxicam were higher than what is accepted as physiologically achievable in patients. Leo cells were most sensitive to (S)-HDAC-42 and Velcade compared to calcitriol and piroxicam.

Genomic imbalances in Leo cells

All of the 50 cells evaluated for chromosome number were hyperdiploid, containing between 120 and 138 chromosomes, with a mean of 131. Seventy-five percent of the cells had a count between 130 and 135. Typical metaphase spreads of Leo cells (Fig. 8Ai,ii) showed that most of the chromosomes were short armed and 6–8 chromosomes were bi-armed. Centromeres were not detected in three chromosomes using BAC clones that were previously shown to hybridize to all canine autosomes, suggesting that these three aberrant chromosomes may contain centromeres from the sex chromosomes (Fig. 8Bi, ii) [18].

DISCUSSION

Understanding the pathogenesis of prostate cancer and development of novel therapeutic agents can be improved with additional unique cell lines and in vivo animal models that mimic the condition in men [7]. Therefore, development of new cell lines and animal models that closely recapitulate the clinical disease in patients are crucial to understand the molecular heterogeneity and pathogenesis of prostate cancer. Dogs not

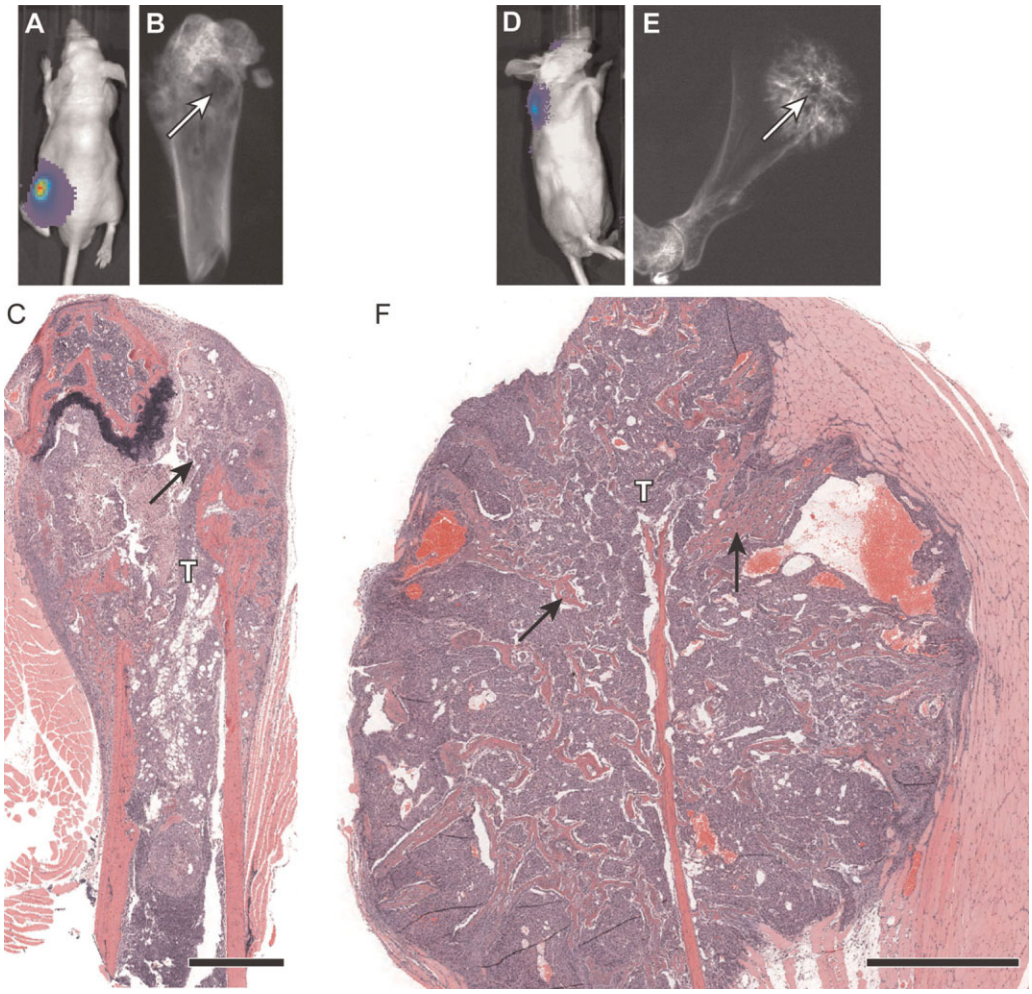

Fig. 6. Evaluation of bone metastasis on day 28 following intracardiac injection of Leo$^{YFP\text{-}Luc}$ in nude mice. **A:** BLI showed metastasis to the left hind limb. **B:** Radiographic evaluation showed osteolysis (arrow) in the metaphyseal region of the humerus. **C:** Histopathologic evaluation showed that tumor (T) replaced bone marrow in the metaphysis and diaphysis of humerus. The metastasis caused extensive bone osteolysis (arrow) characterized by loss of cortical and trabecular bone. *Bar*, 250 μm. Metastasis to the scapula was detected by BLI (**D**). Radiographs demonstrated a radiodense lesion (**E**), which was histologically composed of carcinoma interspersed with radiating trabeculae of woven bone. *Bar*, 250 μm (**F**).

only develop spontaneous prostate cancer but also share similarities to the clinical presentation of prostate cancer in men [2,11,28]. In the present study, we described the establishment of a novel dog prostate cancer cell line (Leo) and characterization of its tumorgenicity and metastatic ability to various organs in nude mice.

The Leo cell line was developed from a 5-year-old castrated male mixed breed dog. The Leo cells formed tumors in the subcutis of nude mice demonstrating its tumorgenicity in vivo. Following intracardiac inoculation, the Leo cells metastasized to multiple sites including the brain, spinal cord, bones, and adrenal gland. The Leo prostate cancer cells exhibited a remarkable tropism for developing metastases in the brain based on the 80% incidence of brain metastases. It has been reported that MMP-9 is up-regulated in most brain metastases [26]. MMP-9 belongs to matrix metalloprotease family of enzymes that degrades the extracellular matrix leading to invasion of tumor cells [29]. High expression of MMP-9 by Leo cells suggests that it might play a significant role in the development of brain metastases. Increased VEGF expression by cancer cells helps in angiogenesis and transendothelial migration by regulating the permeability of brain microvascular endothelial cells [30]. The Leo cells express VEGF, which may be important in the development of brain metastases seen in this model. Although VEGF and MMP-9 may facilitate brain metastasis, other factors must also be involved because the Ace-1 and TCC cell lines also produce VEGF and MMP-9 and do not metastasize to the brain.

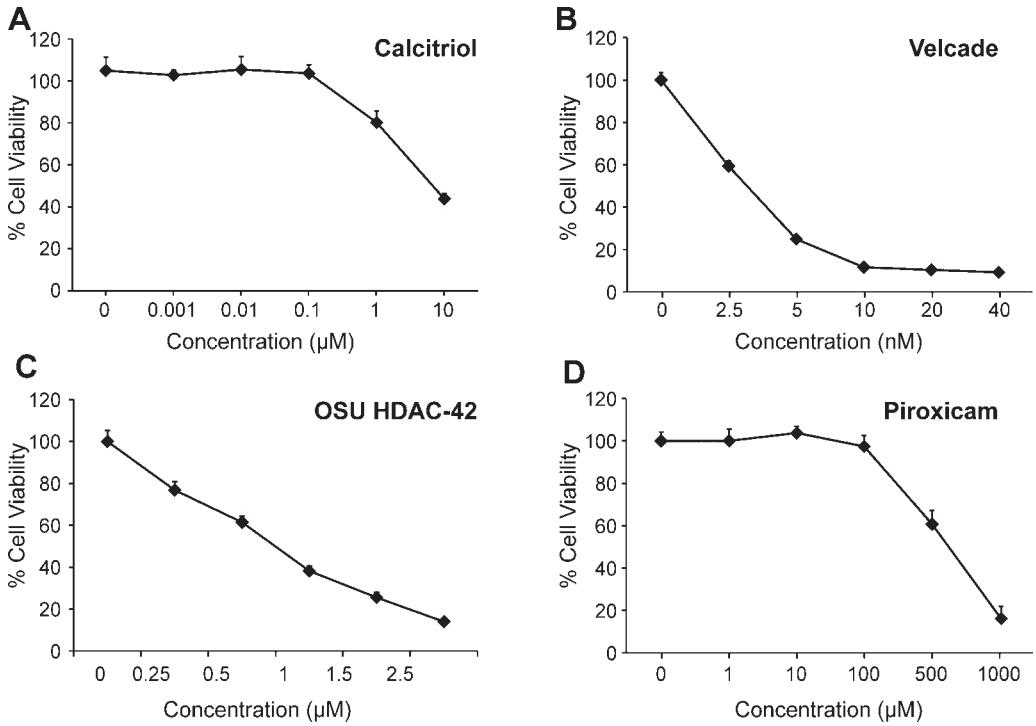

Fig. 7. Dose-response of Leo cell viability to calcitriol (**A**), Velcade (**B**), (S)-HDAC-42 (Ar-42) (**C**) and piroxicam (**D**) treatment. An MTT assay was performed with six replicates for each dose for 72 hr. IC_{50} values for calcitriol, piroxicam, (S)-HDAC-42 and Velcade were 6.8 μm, 518 μm, 0.95 μm, and 1.9 nm, respectively. Bars represent mean + standard deviation of six replicates.

The brain is a rich source of NGF, which is important in the development and maintenance of nervous tissue [31]. NGF regulates its action by binding and activating to two types of neurotrophin receptors, a low affinity nerve growth factor receptor (LNGFR or P75) and NTRK [32]. However, expression of NGF, LNGFR, and NTRK1 were not detectable in Leo cells. Leo cells had severe chromosomal imbalances such as hyperdiploidy and bi-armed chromosomes. Further evaluation of the chromosome imbalances will be important to understand the molecular pathogenesis of metastasis of the Leo cells.

Dog prostate cancers can have mixed histologic features of adenocarcinoma and ductal differentiation [2]. It has been suggested that prostate cancer in dogs may originate from prostate ductal cells that are positive for CK7 [23,24]. Expression of CK7 in addition to secretory epithelial CKs, 8, and 18, by the Leo cells suggests that they have differentiated towards both secretory and ductal cells. Ductal cells with CK7 expression in dogs may also have urothelial differentiation [24].

The AR in dogs is expressed in prostate secretory and basal epithelial cells, ductal cells, stromal cells, and the prostatic urethra [23]. However, in neutered dogs the AR is not expressed. Lack of expression of AR in the Leo cell line, developed from a prostate carcinoma in a neutered dog, is consistent with previous reports and typical of an androgen-insensitive canine prostate carcinoma [23]. The Leo cells were negative for vimentin, which is generally expressed by stromal cells although it has been reported in some prostate cancer cells suggesting epithelial to mesenchymal transition [4]. PSA, a biomarker of prostate cancer in human, is expressed in glandular epithelium and liquefies the semen by degrading semenogelin [33,34]. PSA belongs to the family of kallikrein genes and it is encoded by kallikrein 3. In human 15 kallikreins were identified whereas in dogs only 14 kallikreins are present. The human kallikrein 3 gene encoding PSA in humans is absent in dogs [35]. However, dog kallikrein 2, encoding AE, shares 58% amino acid homology with human PSA and both genes are regulated by androgens [36,37]. Polyclonal and monoclonal PSA antibodies cross-react with human kallikreins 1 and 2 since the degree of amino acid homology is 80% [38]. A few reports have demonstrated staining for PSA (using antibodies to human PSA) in normal dog prostate and canine prostate cancers [39]. Presumably this may be due to cross-reactivity to canine AE. However, since dogs lack a homolog to human PSA, PSA assay and immunohistochemistry generally are not useful in dogs [39]. The Leo cells did express AE.

The bone metastases that developed in nude mice with the Leo cells were predominantly osteolytic

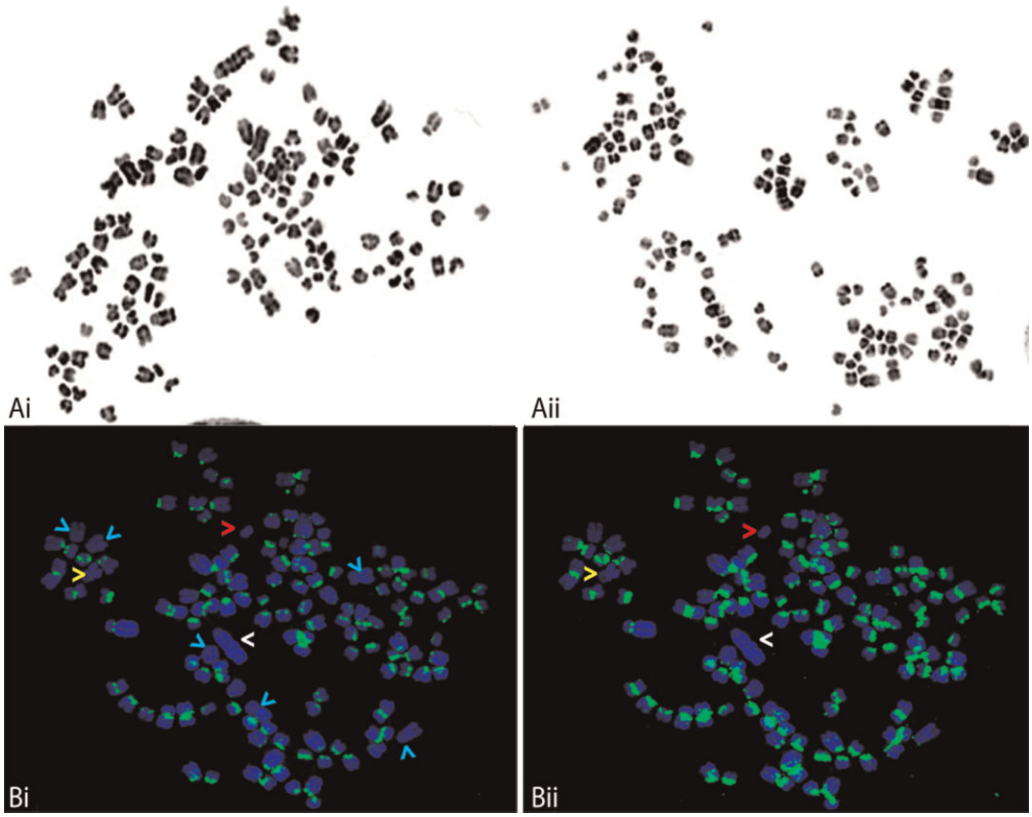

Fig. 8. **A**i,ii: Typical metaphase chromosome preparations derived from Leo cells, exhibiting chromosome numbers in excess of 130 per cell. In addition to the high number of chromosome number, there are several bi-armed chromosomes indicative of structural as well as numerical changes. **B**i: Hybridization of two BAC clones that map to all autosomes of the canine genome revealed that centromeres were detected in all but nine chromosomes (arrows). **B**ii: Overexposure of the same metaphase spreads was unable to detect even a weak signal at the centromeres of three (red, yellow and white arrowheads) of the nine chromosomes.

similar to that observed in the dog with the tibial metastasis. Dog prostate cancer metastases to bones mostly affect the axial skeleton and proximal long bones and can be osteoblastic, osteolytic, or mixed [2]. We have also developed a nude mouse model of dog prostate cancer using the Ace-1 cells that develop a 100% incidence of mixed osteoblastic and osteolytic bone metastases [11]. The Leo cells have a unique metastatic pattern in vivo with a relatively low incidence of metastases to bone (20%). The RANKL and OPG axis has been shown to play an important role in regulating osteolytic bone metastases [40]. RANKL expressed by prostate cancer cells binds to RANK receptor expressed on the surface of osteoclast precursors and induces their differentiation and maturation into active osteoclasts. OPG expressed by cancer cells acts as decoy receptor for RANKL and prevents it from binding to RANK resulting in inhibition of osteoclastogenesis [41]. Leo cells, similar to the Ace-1 prostate cancer cell line, express high levels of both RANKL and OPG. The RANKL may be responsible for the induction of osteoclastic bone resorption, and the amount of OPG is not adequate to inhibit the osteoclastic bone resorption in the metastases. The Leo cells likely do not make significant osteoblastic factors that are a characteristic of the Ace-1 cells.

Velcade (bortezomib), a proteosome inhibitor, was shown to inhibit prostate cancer growth and osteolytic bone metastases in pre-clinical models [42]. Leo cells were very sensitive to Velcade with an IC_{50} of 1.9 nm. Serum concentrations of Velcade in human patients of 40 to 90 ng/L were shown to have anti-tumor activity without serious adverse effects [43,44]. Therefore, it will be important to test the efficacy of Velcade on tumor growth and metastases in the Leo model of prostate cancer. A novel HDAC-42 (Ar-42) inhibitor developed at Ohio State University was very effective in inhibiting the growth of Leo cells in vitro with an IC_{50} of 0.95 μm at after 72 hr of treatment. This novel phenylbutyrate-derived HDAC inhibitor was shown to possess potent anti-tumor activity in prostate cancer by inducing apoptosis [45]. Despite the fact that calcitriol and piroxicam had inhibited the Leo cell growth, the IC_{50} concentrations were too great to achieve relevant serum levels in clinical patients.

One of the most important findings of the Leo xenografts was the consistent and frequent development of brain metastases in nude mice. To our knowledge, this is the first prostate cancer cell line that consistently develops brain metastases in vivo. This provides a unique translational model to investigate the pathogenesis of brain metastases and develop potent therapeutic strategies to treat or prevent brain metastases. Though the incidence of bone metastases was not high, it may be feasible to develop a subline of the Leo cells with a high rate of bone metastases, which would be a valuable model to study the skeletal complications of prostate cancer. Therefore, the new Leo prostate cancer cell line provides a valuable tool to help understand the molecular mechanisms responsible for the pathogenesis of prostate cancer and metastases to the brain and bone.

ACKNOWLEDGMENTS

This work was supported by the National Cancer Institute (2P01 CA93900) and The Ohio State University College of Veterinary Medicine (520026). We thank Tim Vojt for help with preparation of the figures, Wessel Dirksen for help with laboratory experiments and Alan Fletcher for help with the histology.

REFERENCES

1. Jemal A, Siegel R, Ward E, Hao Y, Xu J, Murray T, Thun MJ. Cancer statistics, 2008. CA Cancer J Clin 2008;58:71–96.
2. Waters DJ, Sakr WA, Hayden DW, Lang CM, McKinney LA, Murphy GP, Radinsky R, Ramoner R, Richardson RC, Tindall DJ. Workgroup 4: Spontaneous prostate carcinoma in dogs and nonhuman primates. Prostate 1998;36:64–67.
3. Khanna C, Lindblad-Toh K, Vail D, London C, Bergman P, Barber L, Breen M, Kitchell B, McNeil E, Modiano JF. The dog as a cancer model. Nat Biotechnol 2006;24:1065–1066.
4. LeRoy BE, Thudi NK, Nadella MVP, Toribio RE, Tannehill-Gregg SH, van Bokhoven A, Davis D, Corn S, Rosol TJ. New bone formation and osteolysis by a metastatic, highly invasive canine prostate carcinoma xenograft. Prostate 2006;66:1213–1222.
5. Bubendorf L, Schöpfer A, Wagner U, Sauter G, Moch H, Willi N, Gasser TC, Mihatsch MJ. Metastatic patterns of prostate cancer: An autopsy study of 1,589 patients. Hum Pathol 2000;31:578–583.
6. Harisinghani MG, Barentsz J, Hahn PF, Deserno WM, Tabatabaei S, van de Kaa CH, de la Rosette J, Weissleder R. Noninvasive detection of clinically occult lymph-node metastases in prostate cancer. N Engl J Med 2003;348:2491–2499.
7. Shah RB, Mehra R, Chinnaiyan AM, Shen R, Ghosh D, Zhou M, MacVicar GR, Varambally S, Harwood J, Bismar TA. Androgen-independent prostate cancer is a heterogeneous group of diseases lessons from a rapid autopsy program. Cancer Res 2004;64:9209–9216.
8. Wu S, Jones E, Gulley J, Arlen P, Chen C, Figg W, Dahut W. Routine interval computed tomography in detecting new soft tissue disease in patients with androgen-independent prostate cancer (AIPC) and only bone metastasis. J Clin Oncol 2006; 24:4621.
9. Tremont-Lukats IW, Bobustuc G, Lagos GK, Lolas K, Kyritsis AP, Puduvalli VK. Brain metastasis from prostate carcinoma. Cancer 2003;98:363–3638.
10. Marosi C. Chemotherapy in patients with brain metastases. Mag Eur Med Oncol 2008;1:11–13.
11. Thudi NK, Martin CK, Nadella MVP, Fernandez SA, Werbeck JL, Pinzone JJ, Rosol TJ. Zoledronic acid decreased osteolysis but not bone metastasis in a nude mouse model of canine prostate cancer with mixed bone lesions. Prostate 2008;68:1116–1125.
12. Stone KR, Mickey DD, Wunderli H, Mickey GH, Paulson DF. Isolation of a human prostate carcinoma cell line (DU 145). Int J Cancer 1978;21:274–281.
13. Nadella MV, Kisseberth WC, Nadella KS, Thudi NK, Thamm DH, McNiel EA, Yilmaz A, Boris-Lawrie K, Rosol TJ. NOD/SCID mouse model of canine T-cell lymphoma with humoral hypercalcaemia of malignancy: Cytokine gene expression profiling and in vivo bioluminescent imaging. Vet Comp Oncol 2008;6:39–54.
14. Wright K, El Masri W, Osman A, Roberts S, Trivedi J, Ashton B, Johnson W. The cell culture expansion of bone marrow stromal cells from humans with spinal cord injury: Implications for future cell transplantation therapy. Spinal Cord 2008;46:811–817.
15. Kaewsakhorn T, Kisseberth WC, Capen CC, Hayes KA, Calverley MJ, Inpanbutr N. Effects of calcitriol, seocalcitol, and medium-chain triglyceride on a canine transitional cell carcinoma cell line. Anticancer Res 2005;25:2689–2696.
16. Breen M, Bullerdiek J, Langford CF. The DAPI banded karyotype of the domestic dog (*Canis familiaris*) generated using chromosome-specific paint probes. Chromosome Res 1999;7:401–406.
17. Breen M, Jouquand S, Renier C, Mellersh CS, Hitte C, Holmes NG, Chéron A, Suter N, Vignaux F, Bristow AE. Chromosome-specific single-locus fish probes allow anchorage of an 1800-marker integrated radiation-hybrid/linkage map of the domestic dog genome to all chromosomes. Genome Res 2001; 11:1784.
18. Thomas R, Duke S, Karlsson E, Evans A, Ellis P, Lindblad-Toh K, Langford C, Breen M. A genome assembly-integrated dog 1 Mb BAC microarray: A cytogenetic resource for canine cancer studies and comparative genomic analysis. Cytogenet Genome Res 2008;122:110–1121.
19. Breen M, Hitte C, Lorentzen TD, Thomas R, Cadieu E, Sabacan L, Scott A, Evanno G, Parker HG, Kirkness EF, Hudson R, Guyon R, Mahairas GG, Gelfenbeyn B, Fraser CM, Andre C, Galibert F, Ostrander EA. An integrated 4249 marker FISH/RH map of the canine genome. BMC Genomics 2004;5:65.
20. Irizarry RA, Hobbs B, Collin F, Beazer-Barclay YD, Antonellis KJ, Scherf U, Speed TP. Exploration, normalization, and summaries of high density oligonucleotide array probe level data. Biostatistics 2003;4:249.
21. Smyth GK. Linear models and empirical Bayes methods for assessing differential expression in microarray experiments. Stat Appl Genet Mol Biol 2004;3:1027.
22. Gordon A, Glazko G, Qiu X, Yakovlev A. Control of the mean number of false discoveries, Bonferroni and stability of multiple testing. Ann Appl Stat 2007;1:179–190.
23. Leav I, Schelling KH, Adams JY, Merk FB, Alroy J. Role of canine basal cells in prostatic post natal development, induction of hyperplasia, sex hormone-stimulated growth; and the ductal origin of carcinoma. Prostate 2001;47:149–163.

24. LeRoy BE, Nadella MVP, Toribio RE, Leav I, Rosol TJ. Canine prostate carcinomas express markers of urothelial and prostatic differentiation. Vet Pathol 2004;41:131–140.
25. Chapdelaine P, Gauthier E, Ho-Kim MA, Bissonnette L, Tremblay RR, Dube JY. Characterization and expression of the prostatic arginine esterase gene, a canine glandular kallikrein. DNA Cell Biol 1991;10:49–59.
26. Arnold SM, Young AB, Munn RK, Patchell RA, Nanayakkara N, Markesbery WR. Expression of p53, Bcl-2, E-cadherin, matrix metalloproteinase-9, and tissue inhibitor of metalloproteinases-1 in paired primary tumors and brain metastasis. Clin Cancer Res 1999;5:4028–4033.
27. Yano S, Shinohara H, Herbst RS, Kuniyasu H, Bucana CD, Ellis LM, Davis DW, McConkey DJ, Fidler IJ. Expression of vascular endothelial growth factor is necessary but not sufficient for production and growth of brain metastasis 1. Cancer Res 2000;60:4959–4967.
28. Teske E, Naan E, Van Dijk E, Van Garderen E, Schalken J. Canine prostate carcinoma: Epidemiological evidence of an increased risk in castrated dogs. Mol Cell Endocrinol 2002;197:251–255.
29. Nathoo N, Chahlavi A, Barnet GH, Toms SA. Pathobiology of brain metastases. Br Med J 2005;58:237–242.
30. Lee TH, Avraham HK, Jiang S, Avraham S. Vascular endothelial growth factor modulates the transendothelial migration of MDA-MB-231 breast cancer cells through regulation of brain microvascular endothelial cell permeability. J Biol Chem 2003; 278:5277–5284.
31. Misko T. Nerve growth factor in neuronal development and maintenance. J Exp Biol 1987;132:177–190.
32. Bothwell M. Functional interactions of neurotrophins and neurotrophin receptors. Annu Rev Neurosci 1995;18:223–253.
33. Hernandez J, Thompson IM. Prostate-specific antigen: A review of the validation of the most commonly used cancer biomarker. Cancer 2004;101:894–904.
34. Robert M, Gibbs BF, Jacobson E, Gagnon C. Characterization of prostate-specific antigen proteolytic activity on its major physiological substrate, the sperm motility inhibitor precursor/ semenogelin I. Biochemistry 1997;36:3811–3819.
35. Elliott MB, Irwin DM, Diamandis EP. In silico identification and Bayesian phylogenetic analysis of multiple new mammalian kallikrein gene families. Genomics 2006;88:591–599.
36. Dube J. Search for androgen response elements in the proximal promoter of the canine prostate arginine esterase gene. J Androl 1995;16:304–311.
37. Clements J. The glandular kallikrein family of enzymes: Tissue-specific expression and hormonal regulation. Endocr Rev 1989; 10:393–419.
38. Yousef GM, Diamandis EP. An overview of the kallikrein gene families in humans and other species: Emerging candidate tumour markers. Clin Biochem 2003;36:443–452.
39. Lai CL, van den Ham R, van Leenders G, van der Lugt J, Mol JA, Teske E. Histopathological and immunohistochemical characterization of canine prostate cancer. Prostate 2008;68:477–488.
40. Wittrant Y, Theoleyre S, Chipoy C, Padrines M, Blanchard F, Heymann D, Redini F. RANKL/RANK/OPG: New therapeutic targets in bone tumours and associated osteolysis. Biochimica Biophysica Acta-Rev Cancer 2004;1704:49–57.
41. Zhang J, Dai J, Yao Z, Lu Y, Dougall W, Keller ET. Soluble receptor activator of nuclear factor κB Fc diminishes prostate cancer progression in bone. Cancer Res 2003;63:7883–7890.
42. Whang P, Gamradt S, Gates J, Lieberman J. Effects of the proteasome inhibitor bortezomib on osteolytic human prostate cancer cell metastases. Prostate Cancer Prostatic Dis 2005;8:327–334.
43. Moreau P, Coiteux V, Hulin C, Leleu X, van de Velde H, Acharya M, Harousseau JL. Prospective comparison of subcutaneous versus intravenous administration of bortezomib in patients with multiple myeloma. Haematologica 2008;93:1908–1911.
44. Attar EC, DeAngelo DJ, Supko JG, D'Amato F, Zahrieh D, Sirulnik A, Wadleigh M, Ballen KK, McAfee S, Miller KB. Phase I and pharmacokinetic study of bortezomib in combination with idarubicin and cytarabine in patients with acute myelogenous leukemia. Clin Cancer Res 2008;14:1446–1454.
45. Kulp SK, Chen CS, Wang DS, Chen CY, Chen CS. Antitumor effects of a novel phenylbutyrate-based histone deacetylase inhibitor,(S)-HDAC-42, in prostate cancer. Clin Cancer Res 2006;12:5199–5206.